1. From models to materials. Mutations and extensions in DFT & LF modeling strategies. (O1-part2)

The relevant systems in practical luminescence applications belong, theoretically, to solid state problems, and the electronic structure approach in this field is dependent on DFT (Density Functional Theory) methods. In the attempt to consider the lanthanide systems by DFT methods in the solid state (band calculations), we run into a fundamental impediment. Namely, the groundstates of the lanthanide systems are quasi-degenerate. Most of the free ions present degenerate ground terms (with the exception of the f^7 configuration, with the ^8S ground state), and the f shell of the lanthanide ions in compounds is only slightly perturbed, compared to the free ions. This situation warns against using DFT for lanthanide materials

On the other hand, the practice of band DFT calculations, of smearing the electronic population in the frontier bands, fortunately saves the relevance of DFT. Namely, the invalidation of DFT for degenerate ground states in atomic or quasi-atomic systems (such as lanthanides in compounds) is determined by the angular part of the central wave function (allowing variations of the density maps, at zero or low energy cost). The band equalization of the electronic population of the quasi-degenerate states quenches the angular degrees of freedom. Thus, it seems that band structure techniques with plane waves can describe well the electronic structure of lanthanide compounds, at least at the orbital level.

Another impediment of DFT is the impossibility of calculating the excited spectral states, as would be necessary in the explanation and prediction of luminescence properties. Note that the Time-Dependent DFT alternative is limited only to single-electronic excitations, ignoring the multi-particle components. The complete spectral simulation requires, in addition to the data of orbital energies (of mono-electronic nature) and inter-electronic parameters. The analyzes and procedures presented here provide an alternative methodological path that can open the DFT pathway in spectroscopic objectives. We have developed a way to extract Slater-Condon (SC) parameters from pseudopotential files through a dedicated analysis of plane wave calculations. The technical solution consists in fitting the atomic radial parts from the pseudo-potential with STO type primitives (Slater-type orbitals), followed by the analytical evaluation of the SC integrals. We thus obtain data for free atoms and ions.

To obtain radial profiles assignable to f and d shells, we performed the non-routine treatment described in the following. Taking optimized LnF_3 cells, we did a Gamma-only calculation, allowing spin polarization in an unrestricted regime, while still imposing a spinless restricted-type scheme. This numeric experiment implied fractional equal occupations on all f-type orbitals, i.e., seven spin-up bands and seven spin-down ones. More concretely, having a lanthanide with f^n configuration, then, each f-type unrestricted band gets the $n/14$ occupation. The fractional occupations are allowed in conceptual DFT and implemented in the controls of the used code. It happens that these functions, corresponding to the partly filled f orbitals, are at the top of the occupied bands sequence. Then, the black-box data from this calculation (converged wavefunctions, potential, and charge distribution) are used as the starting point for subsequent non-iterative jobs. To get the f function, the occupation is set to represent the realistic spin polarization of the free-ion ground state. Thus, if the f population consists of n_α spin-up and n_β spin-down electrons, it must input seven $n_\alpha/7$

and, respectively, seven $n_\beta/7$ fractional values in the corresponding occupations of unrestricted orbital stacks.

Then, a spin polarization density cube carrying the (n_α-n_β) total of unpaired electrons is produced. This cube is handled with our own fortran code, which produces an averaged radial profile around the targeted lanthanide center. More concretely, one fixes a r_{max} maximal radius and a number of desired intervals, N_{max}, having the $dr= r_{max}/N_{max}$ width. Each point of the cube having the distance from the lanthanide center comprised between $dr\cdot(i$-1) and $dr\cdot i$ is collected, performing, at the end, the average of the radial lengths and corresponding f-type spin densities which are falling the i-th interval. The equal averaging of spin-orbital populations emulates a quasi-spherical nature of the lanthanide center, with the spin density being proportional to the squared radial profile, $r^2R_{4f}^2$. The averaged 4f wavefunction is easily obtained by taking the square root, since the 4f radial part does not show nodal points.

Things are a bit more complicated for the extraction of the 5d function. Starting with a wavefunction from the first enforcedly restricted calculations, we did a non-iterative run for an artificial configuration looking like $f^{n-1}d^1$ orbital promotion, keeping the f electrons in restricted shape, while the d-type electron is polarized as spin-up. To identify the former empty orbitals, having the preponderant 5d character, one must run preliminary the analysis revealing the atomic composition of the bands. Thus, all the f-type highest occupied orbitals, both α and β, have equal (n-1)/14 occupation numbers, whilst five upper spin-up orbitals get the 0.2 population, corresponding to the shell-averaged d^α electron from the $f^{n-1}d^1$ configuration. In this way, by doing the cube of spin density and the corresponding directional averaging, one obtains the profile corresponding to the squared d-type function, $r^2R_{5d}^2$. This has three peaks, bigger towards a larger radius. To obtain the 5d function, one must take the square root and assign the corresponding signs (since the minima between peaks are nodal points). We put the plus sign for the domains of inner and outer peaks, with the middle one being taken as negative. Examples of radial profiles for the functions f and d in the free ion, compared to the one included in the network, can be seen in Figure 1. From the radial profiles obtained after the above description, the Slater-Condon parameters can be extracted, following the procedure described in the previous stage of the project.
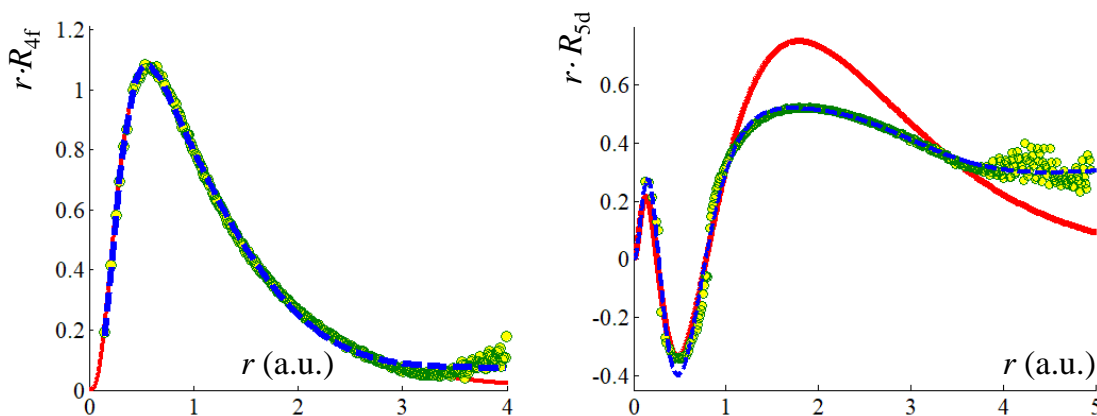

Figure 1. Comparison of radial profiles of 4f and 5d-type orbitals for the free Gd^{3+} and for the ion in the idealized GdF_3 cubic lattice. Left panel: f-type functions; Right side: d-type functions. The continuous lines (red) correspond to the numeric DFT calculations with ATOMPAW, for the charged atom. The circles stand for the points collected from plane-wave calculations on GdF_3, while the dashed line corresponds to the fit of these sets with STO primitives.

One notices that, while the 4f peaks from the two cases are closely similar, the 5d case shows sensible differences. This can be explained by the fact that the f electrons, although important for optical and magnetic properties, are not participating in the bonding. Contrary to this, the 5d virtual of the free ion are strongly involved in the bonding, acting as acceptors of the density donated by the ligands. The points collected from handling the computed spin density cubes are shown with circles. The puckered distribution, at large distances, is due to the deviation from spherical symmetry, in the lattice environment of the central ion.
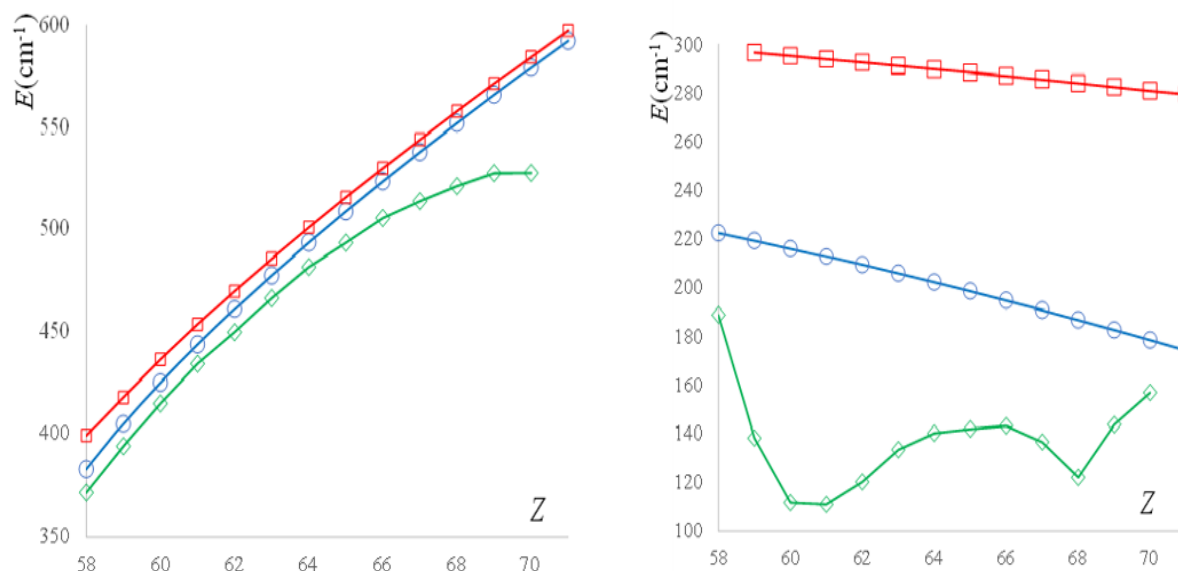

Figure 2. The variation of the F_2^{ff} (left side panel) and F_2^{fd} (right side panel) intra-shell parameters along the lanthanide series. The blue line (circle symbols) corresponds to the shells of neutral atoms, extracted from pseudopotential. The red line (square symbols) stands for the triple ionized lanthanides, Ln^{3+}, computed with the ATOMPAW pseudopotential generator. The green line (diamond symbols) corresponds to the fit on the radial pattern averaged from calculations on LnF_3 structures, idealized as cubic cells .

In LnF_3, one obtains a general lowering of the integrals, below the values for free ions, even below those of the neutral atoms. This is due to the so-called nephelauxetic effect, whose etymology suggests an inflation of atomic radial profiles. Since the f shell is only slightly changed by the immersion of the ionic body in a lattice, the nephelauxetic reduction is small. The averaged nephelauxetic ratio, $\beta^{ff} = F_k^{ff}(LnF_3)/F_k^{ff}(Ln^{3+})$, taken on all k=0, 2, 4, 6 indices and all lanthanide ions, is about $\beta^{ff} \approx 0.95$, in line with the close similarity of 4f profiles from the left side of Figure 2. On the contrary, as shown on the right side of Figure 2, the d shell undergoes strong inflation, with amplitude attenuated at the former ionic radius and moved towards the ligands. As a consequence, the averaged nephelauxetic ratio for the 5d functions is strongly sub-unitary, $\beta^{dd} \approx 0.38$. Combining the different behavior of the f and d shells, the nephelauxetic ratio of the F_k^{fd} integrals leads to an intermediate value, with $\beta^{fd} \approx 0.72$.

Having the Slater-Condon parameters from data specific to the DFT treatments used, further, in Ligand Field (LF) type models, we made an innovative methodological extension, hybridizing a computational procedure and a phenomenological model. Along this path, numerical experiments innovatively designed within DFT, allow the advancement towards the modeling of complete spectra.

2. New perspectives and prospective investigations in lanthanide-based phosphorescent materials. Selected case studies (O2-part1)

In this thematic area, we carry out a comprehensive approach, of critical verification and methodological innovation, progressively advancing towards understanding the mechanisms, analysis and prediction of optical properties. Proceeding systematically, I first consider a very simple model, in order to clearly identify and express the related factors.

We consider $[TbF]^{+2}$ model system in CASSCF calculations, including eight electrons in seven orbitals, CASSCF(8,7). The Tb–F distance is conventionally set to 2.35 Å, corresponding to the range encountered in various solid-state fluorides. The CASSCF-computed states assignable to the $^7\Phi$, $^7\Delta$, $^7\Pi$, and $^7\Sigma$ spectral terms, ordered in this sequence, have the relative energies 0.0, 497.5, 1008.7, and 1339.8 cm^{-1}, respectively. Figure 3 depicts the computed levels and suggests the relationship with the orbital LF scheme, depicting the canonical MOs, which is practically almost pure AOs, which can be described as the location of the β electron for the given spectral term. In this simple case, the terms are parallel to the itinerant f^β component from the $f^8 \equiv f^{7\alpha}f^\beta$ configuration of Tb(III). The scheme also suggests the meaning of the AOM-type parameterization, namely, the relative magnitudes of the e^f_σ, e^f_π, and e^f_δ perturbations for f electrons, after conventionally setting the $e^f_\varphi = 0$ energy origin. The above energy levels were obtained in the primary active space of CASSCF(8,7), related to the f^8 configuration. Extending the space to also comprise the five d-type virtual orbitals to CASSCF(8,12), the split of ^7F term is slightly modified, with the results being interpreted as the following AOM parameters: $e^f_\sigma(F) = 1175.0$ cm^{-1}, $e^f_\pi(F) = 910.2$ cm^{-1}, and $e^f_\delta(F) = 466.5$ cm^{-1}, in addition to the imposed $e^f_\varphi = 0$. Note that the e_δ parameter is not negligible, as customary in the established AOM practice, presuming e^f_δ and e^f_φ are null, because the ligands are not expected to be able to exert δ and φ true orbitals overlap.
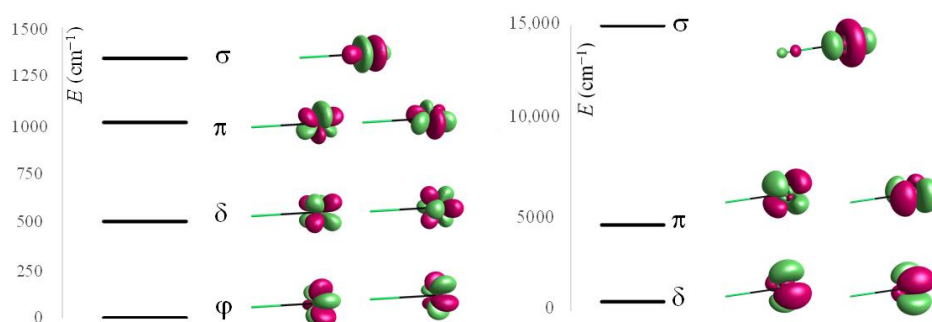

Figure 3. The left side: Computed relative energies of $^7\Phi$, $^7\Delta$, $^7\Pi$, and $^7\Sigma$ spectral terms resulting from the LF split of the ^7F ground state of Tb(III) in $[TbF]^{+2}$ and relationship with the f-type LF scheme, labeled by φ, δ, π, and σ representations of f orbitals in the axial symmetry. The right side: Computed relative energies of $^7\Delta$, $^7\Pi$, and $^7\Sigma$ spectral terms resulting from the LF split of the ^7D excited state of Tb(III) in $[TbF]^{+2}$ and relationship with the d-type LF scheme, labeled with the δ, π, and σ representations of d orbitals in the axial symmetry. The isosurfaces are drawn at a 0.1 e/Å³ threshold.

The Tb(III) ion is also well suited to discuss the d-type ligand field in lanthanides, analyzing the $f^8 \rightarrow f^7d$ orbital promotions (implying 5d empty AOs) in the CASSCF(8,12) setting. The f^7 subconfiguration is spherically symmetric, the set of f^7d excited states then has D representation, and the spectrum is parallel with the LF scheme of d electrons. In more detail, there is a ^7D term arising from the $f^{7\alpha}d^\beta$ configuration and a ^9D term arising from the

spin swap to $f^7\alpha d^\alpha$. The high-spin states are lower in energy, benefiting from stabilization by the f–d inter-hell exchange coupling. In the following, as a measure of the d-type LF split, we consider the spin-septet terms, keeping the same multiplicity as in the ^7F ground state. To be distinguished from the d-type LF encountered in transition metal complexes, here, we deal with an excited-state d orbital population. In linear symmetry, the ^7D term splits into $^7\Delta$, $^7\Pi$, and $^7\Sigma$ levels. Shifting the $^7\Delta$ orbital doublet to zero, namely, imposing $e^d_\delta = 0$, the relative gaps can be assigned to the d-type AOM parameters, resulting in $e^d_\sigma(F) = 14{,}959.7$ cm^{-1} and $e^d_\pi(F) = 4518.9$ cm^{-1}.

The following numeric experiment demonstrates the variation in the computed spectral terms in the $[TbF_2]^+$ unit as function of the F–Tb–F angle, which we performed to check whether the geometry dependence follows the pattern of the angular overlap model version of ligand field theory. Figure 3a shows the computation data with open circles and the fitted AOM variation with a continuous line. The adjusted parameters, accounting for the whole variation, are $e^f_\sigma(F) = 1341.7$ cm^{-1}, $e^f_\pi(F) = 1018.6$ cm^{-1} , and $e^f_\delta(F) = 514.3$ cm^{-1}. The CASSCF and AOM data were fitted in their barycenters for better visualization. The fit is quite good in the 90°–180° domain of the F–Tb–F angles, with the deviation at lower angles being pardonable because it enforces the strong ligand–ligand repulsion, and the small inter-ligand angles are avoided in real lanthanide chemistry. The conclusion that the AOM pattern is satisfactorily obtained with the calculation also holds for the d-type LF, represented in Figure 3b. The parameters giving an overall satisfactory fit to the d-LF angular variation are $e^d_\sigma(F) = 8356.6$ cm^{-1} and $e^d_\pi(F) = 3690.5$ cm^{-1}, with a constrained $e^d_\delta(F) = 0.0$.
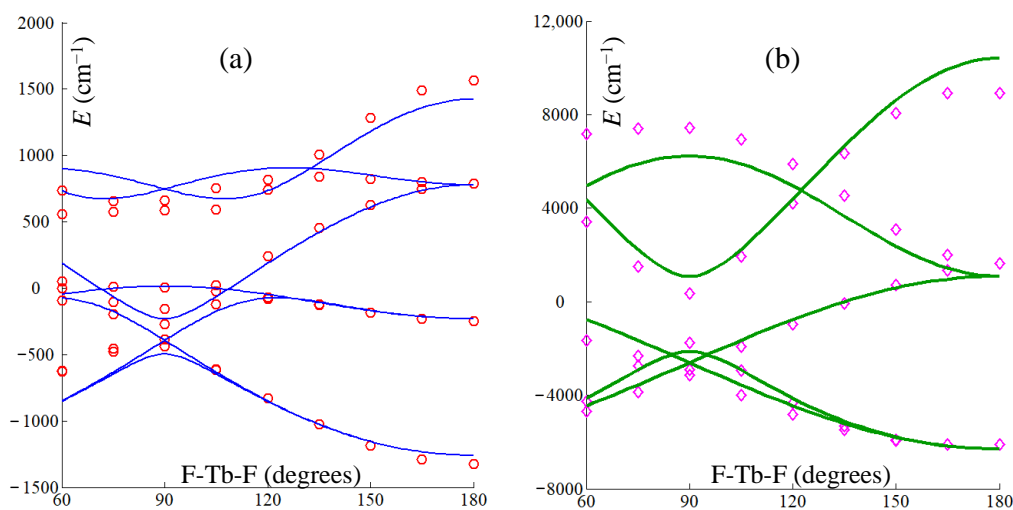

Figure 4. The variation as a function of F–Tb–F angle of computed spectral terms (marked points) and fitted AOM eigenvalues (continuous lines) in the $[TbF_2]^+$ unit. (**a**) The left side represents the LF split of the ^7F term and the f-type LF scheme; (**b**) the right side shows the ^7D and d-type LF scheme. The energy sets are drawn with their barycenter in the origin of the energy scale.

The next systematic step approaches the octahedral $[TbF_6]^{-3}$ unit. According to AOM, the octahedral LF eigenvalues can be written as follows:

$$\varepsilon(a_{2u}) = 6e_\delta; \qquad \varepsilon(t_{1u}) = \frac{5}{2}e_\varphi + \frac{3}{2}e_\pi + 2e_\sigma \ ; \qquad \varepsilon(t_{2u}) = \frac{3}{2}e_\varphi + 2e_\delta + \frac{5}{2}e_\pi \qquad (1)$$

Inserting previously ascribed the $e^f_\lambda(F)$ values from the CASSCF(8,12) calculation on $[TbF]^{+2}$, we predicted values of 916.3 cm^{-1} and 409.5 cm^{-1} for the $\Delta_1 = \varepsilon(t_{1u}) - \varepsilon(a_{2u})$ and $\Delta_2 = \varepsilon(t_{2u}) - \varepsilon(a_{2u})$ gaps, respectively. The calculation of the $[TbF_6]^{-3}$ unit, in settings similar to

those of the diatomic metal–ligand system, gives $\Delta_1 = 762.9$ cm^{-1} and $\Delta_2 = 291.9$ cm^{-1}, which are roughly comparable to the result assuming the transferability of the AOM parameters. The discrepancy is explained by the different balances in the non-LF effects subsisting in the positively charged artificial diatomic system versus the negatively charged larger system. The AOM practice does not consider the octahedral gaps with the full set of $\{e_\sigma, e_\pi, e_\delta, e_\varphi\}$ parameters, being confined only to the $\{e_\sigma, e_\pi\}$ couple, first by the empirical assumption that the effects of δ and φ are not chemically intuitive and then by the pragmatic reason that the available data do not allow obtaining a full parametric scheme. Thus, if we consider that the two gaps for the $[TbF_6]^{-3}$ unit are fitted only in the σ-π scheme, we obtain $e_\sigma = 293.9$ cm^{-1} and $e_\pi = 116.7$ cm^{-1}, which is in a range compatible with the experimental spectroscopy [42,76]. Although the chemical intuition may refute the φ and δ bonding effects, the electrostatics support their underground action. However, we leave this matter as a challenge open to further debate. We honestly admit that the calculations have certain limitations; from a different perspective, they can offer more details than are available from experiments.

In another systematic approach, we re-tested the electrostatic hypothesis, in relation to the ab intio results, obtaining surprising results. Thus, in the purely electrostatic hypothesis, the f levels have the following expressions:

$$\varepsilon_\sigma = b_0 + \frac{4}{15} b_2 + \frac{2}{11} b_4 + \frac{100}{429} b_6 \quad \varepsilon_\pi = b_0 + \frac{1}{5} b_2 + \frac{1}{33} b_4 - \frac{25}{143} b_6 ,$$

$$\varepsilon_\delta = b_0 - \frac{7}{33} b_4 + \frac{10}{143} b_6 \quad \varepsilon_\varphi = b_0 - \frac{1}{3} b_2 + \frac{1}{11} b_4 - \frac{5}{429} b_6 \tag{2}$$

where the b_k parameters are

$$b_k(L) = q_L \int_{r=0}^{\infty} (R(r))^2 \frac{min(r,R_L)^k}{max(r,R_L)^{k+1}} r^2 dr = \sum_{i=1}^{n_f} \sum_{j=1}^{n_f} c_i \cdot c_j \cdot N_i \cdot N_j \cdot \left(\frac{1}{R_L^{k+1}} \cdot P_{ij} + R_L^k \cdot Q_{ij} \right), \tag{3}$$

depending entirely only on the orbital part of the metal ion. An important result is the fact that we have developed analytical formulas for these components, depending on the elements of the Gaussian basis (GTO -Gaussian Type Orbitals), functions of exponential parameters ζ and coefficients called contraction, c. The above terms are developed as:

$$P_{ij}^{GTO} = \frac{1}{2} (\zeta_1 + \zeta_2)^{-\frac{1}{2}(n_1+n_2+k+1)} \left(\Gamma\left[\frac{1}{2}(n_1+n_2+k+1), 0\right] - \Gamma\left[\frac{1}{2}(n_1+n_2+k+1), (\zeta_1+\zeta_2)R_L^2\right] \right),$$

$$Q_{ij}^{GTO} = \frac{1}{2} (\zeta_1 + \zeta_2)^{\frac{1}{2}(k-n_1-n_2)} \Gamma\left[\frac{1}{2}(n_1+n_2-k), (\zeta_1+\zeta_2)R_L^2\right] , \tag{4}$$

where Γ are the Gamma incomplete functions.

We checked the pure electrostatic approximation of the LF parameters for the STO-type ZORA/TZ2P basis used in the calculations in Section 3.2. This basis is defined by $\zeta = \{10.2, 4.9, 2.15, 1.65\}$ exponent parameters in Bohr^{-1} and the $n = \{4,4,4,5\}$ sequence of power factors. The BLYP calculation of the free Tb(III) ion provides $c = \{0.405816, 0.614349, 0.227727, -0.0382306\}$ coefficients. The STO-based estimation yields $b_0 = 49{,}421.5$ cm^{-1}, $b_2 = 2257.0$ cm^{-1}, $b_4 = 271.2$ cm^{-1}, and $b_6 = 67.3$ cm^{-1}, which are just a bit larger than the results from GTO. With this, we derive the following parameters: $e_\sigma = 1395.3$ cm^{-1}, $e_\pi = 1176.3$ cm^{-1}, and $e_\delta = 675.64$ cm^{-1} if conventionally considering $e_\varphi = 0$.

Surprisingly, by the roughest approximation of the crystal field, the results are compatible with those of high-level multiconfigurational calculations. This contradicts the long-held belief about the failure of the pure electrostatic approximation in ligand field problems. In fact, the description of the pure electrostatic paradigm was originally related to d-type LF systems, where partial covalent bonds do occur in coordination compounds. In contrast, the lanthanide compounds are more ionic and therefore more suitable for the initial ideas of the electrostatic crystal field. These results, corroborated, suggest the possible design of simplified approaches, usable in complicated situations, a fact demonstrated in a later example (see the discussion around figure 6).

In the following we enter the full complexity of the problems, approaching systems of Tb(III) doped in K_2GdF_5 networks, for which the experimental data suggest interesting optical properties, due to the orbital promotion $f^8 \rightarrow f^7d$. For comparison, we also considered the hypothetical situation of doping in K_2LuF_5, in order to have a benchmark with a diamagnetic host network. Using the Quantum Espresso code, we performed band calculations, with plane wave bases for the valence functions and pseudo-potentials for the atomic nuclei. The code has a very useful option for the problem in question, allowing the emulation of an orbital promotion state, through the artifice of doubling the Fermi level, thus enforcing the prohibition of considering excited states in DFT. The calculation optimizes the fractional orbital populations of the border bands, proposing a valence-conduction redistribution that would correspond to the first excited state. In addition, it is possible to optimize the geometry of the system, both of the crystal cell and the positions of the atoms, in the ground state and in the orbital promotion simulation.

We get a very interesting result. Although the cell increases incrementally, after the promotion of electrons from the valence band to the conduction band, the metal-ligand distances appear slightly contracted in the excited form. This is contrary to the situations known from luminescence studies on molecular, covalent systems. Namely, the excitation is associated with the acquisition of an anti-bond portion, from the transmutation of the existing bond contributions in the fundamental form, this attracting - in general - the tendency to increase the bond distances. By studying the details of the calculation data, we identified the mechanism of this result.

The f electrons, although they determine the optical and magnetic properties, do not contribute to the chemical bond. Instead, the connection in the lanthanide systems is practically ensured by the virtual orbitals of origin 5d, which function as acceptors of the density donated by the ligands. Such a mechanism is well known for transition metals, but it was not taken into consideration as relevant for lanthanides, the obvious fact here being that it is the very mechanism of formation and stabilization of lanthanide compounds. During $f^8 \rightarrow f^7d$ excitation. an f electron, initially inactive in the bonding mechanism, acquires, in the d orbital, incidence in this sense, indirectly. Namely, it exerts a spin polarization on the ligand, so that the dative bond in which the d orbitals were involved acquires the partial character of a covalent spin coupling bond, strengthening the cohesion of the system. Such behavior has not been studied in such terms, until here.

Figure 5 illustrates the modeling data for Tb@ K_2GdF_5 doping, at high concentration in the left and middle parts of the synopsis and low in the right panel. The excited state could only be emulated for the simpler, high-concentration system. We highlight the discussed geometry variations, small but obvious: Tb-F distances between 2.23-2.33 Å for the cell in the ground state and 2.18-2.29 Å for the excited system. The density of states (DOS- Density of States) curves highlight the subtle difference between spin orbitals α (in blue) vs. β (in red), due to the net spin polarization α. Specific excitation differences are visible in the rescaled segments: in (c) the negative peak is attributable to the ⊚ electron from the $f^8 = f^{7\alpha}f^\beta$ configuration of Tb(III), and the pattern with two positive and one negative peaks in (c') suggests that the promotion orbital occurs predominantly in the positive spin pendant, $f^8d = f^{6\alpha}f^\beta d^\alpha$.
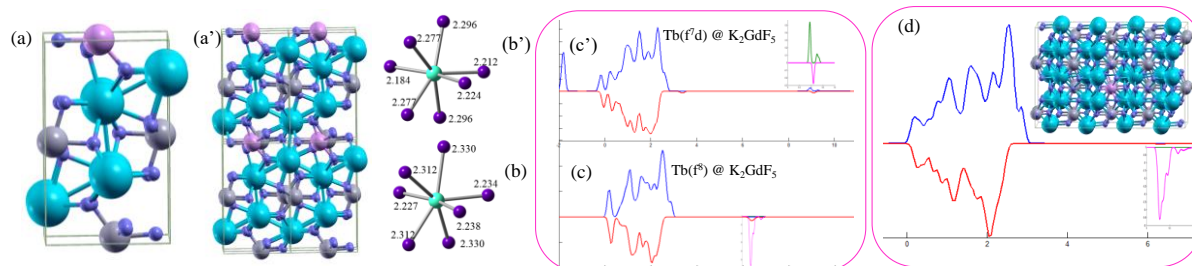
Figure 5. (a) elementary cell and (a') multiplied cell of Tb@K_2GdF_5 system with Tb=25% concentration; (b) and (b') the optimized geometries in ground state Tb(f^8), respectively excited state Tb(f^7d); (c) and (c') density of states (DOS) diagrams for the respective specified situations; (d) enlarged unit cell and DOS results for the extended system, with Tb(f^8), in 2.5% concentration.

Although the modeling of the f→d orbital promotion behavior is well reproduced in the band calculations, the useful information for the crystal field modeling was not properly found in the orbital energies of the band system. Namely, although the population analysis of the band components shows successive groupings of states assimilable with the f states, the orbital energies achieve exaggerated overestimations of the splitting in the ligand field. In this context, given that we are dealing with fluorides, for which the previous analysis revealed that the electrostatic approximation can work surprisingly well, we proceeded to exploit this premise, as an alternative variant of LF modeling. Figure 6 shows the process of selecting clusters of increasing size, with the terbium ion in the center, for which we applied the electrostatic evaluation, the perturbations of each node being factored by the formal charge of the ion. In this way, we also consider the whole positive charges on the ions (K^+) and (Gd^{+3}), in addition to those of the anionic ligands (F^-), the cations generating inverted LF splitting tendencies compared to the anions.
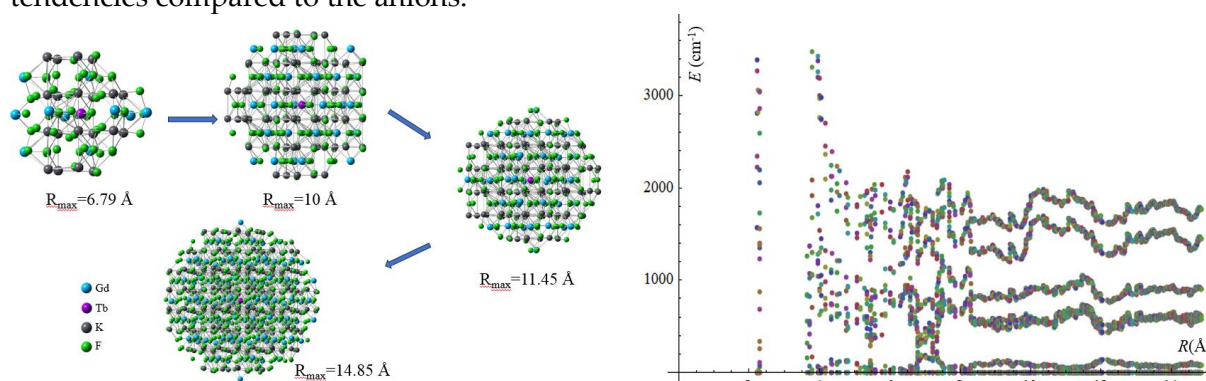

Figure 6. Purely electrostatic treatment of ligand field splitting (LF) for f orbitals in the central Tb(III) ion in a progressively extended nanoscale surround cut from the K_2GdF_5 lattice. On the left, the structures of selected units at different radii. On the right, the Ligand Field energy scheme depending on the progressive collection of new ions, as the cluster radius increases.

In figure 6, we can see, on the left, different dimensions of the crystal cut-out, on the right representing the successive LF scheme obtained when the radius increases. We note a strong variation of the orbital energies, up to large radii, of 8 Å, followed by a relative stabilization. The fact that the distance terms do not attenuate more strongly is somewhat unexpected. For example, it is well known that the Madelung potential is not convergent in direct summation, because it depends in the form $1/R$ on the distance, while the volume increases as R^3, the cumulation in 3D space having the pattern R^2. However, since the electrostatic LF terms, bk,

discussed above, vary in the form $1/R^{k+1}$, and $k>3$, their summation is expected to converge rapidly. Convergence is achieved, but at large radii, which suggests that LF problems can include terms usually neglected by considering the first crystalline surround. Apparently, the direct result, displayed on the right side of figure 6, is an overestimation, obtaining a total splitting of approximately 2000 cm^{-1}, expecting, according to the experiment, values around 700 cm^{-1}. The overestimation results from the use of formal, integer ionic charges. Considering the atomic charges calculated by electronic structure methods, we achieve a reduction by a factor of 0.3, which brings the LF estimate into a reasonable range.
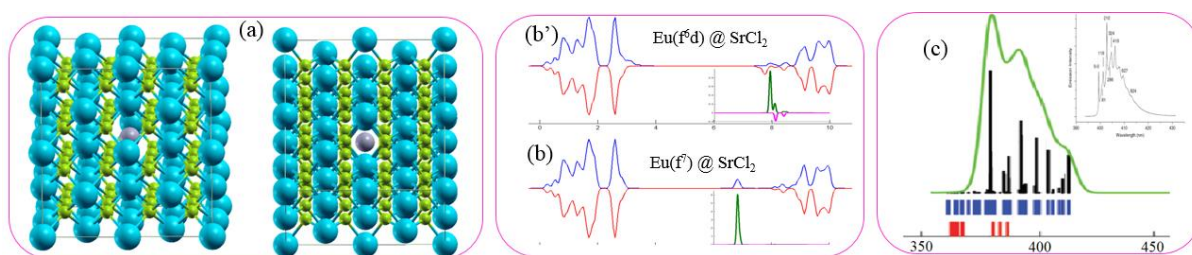

Figure 7. The Eu@ScCl$_2$ system: (a) the cell with the doped ion in the center; (b) and (b') the density of states (DOS) in ground and excited state; (c) Simulation of the convolution of the f-d transitions (as inset, the experimental spectrum).

We also add a brief description of the modeling started in studying the luminescence of divalent europium doped in SrCl$_2$ cubic network. The system and the treatments applied are outlined in Figure 7. The optimization of the crystal geometry for an extended cell (corresponding to a ~2% doping level) with the Eu(II) ion in the center was achieved. We obtain the same trend described before: the reduction of the coordination distance following f$\rightarrow$d excitation. Thus, the first coordination sphere, {EuF$_8$}, has Eu-F bond lengths of 3.0436 Å in the ground state, and 3.121 Å in the excited state. In this case we obtain, from the orbital energies and the total energies of the band calculations, reasonable parameters for the field scheme of the ligands. Adding the Slater-Condon parameters obtained through the original procedure opened in the first part, we achieve a simulation of the luminescence properties, relatively close to the experimental data.

3. Calculations of multi-determinant wave functions on lanthanide cluster models. (O3-part1)

The band treatments, via DFT, described previously, are practically indispensable in the attempt to optimize the geometry of doped systems, and the modeling itself is a valuable way to achieve this goal, providing microscopic details inaccessible experimentally. However, since the DFT approach has intrinsic limitations, the description via multi-configurational methods from Wave Function Theory (WFT) is preferable, whenever possible, namely when the system is molecular (discrete coordinate unit), or if a decoupling of cluster type, from the crystalline arrangement.
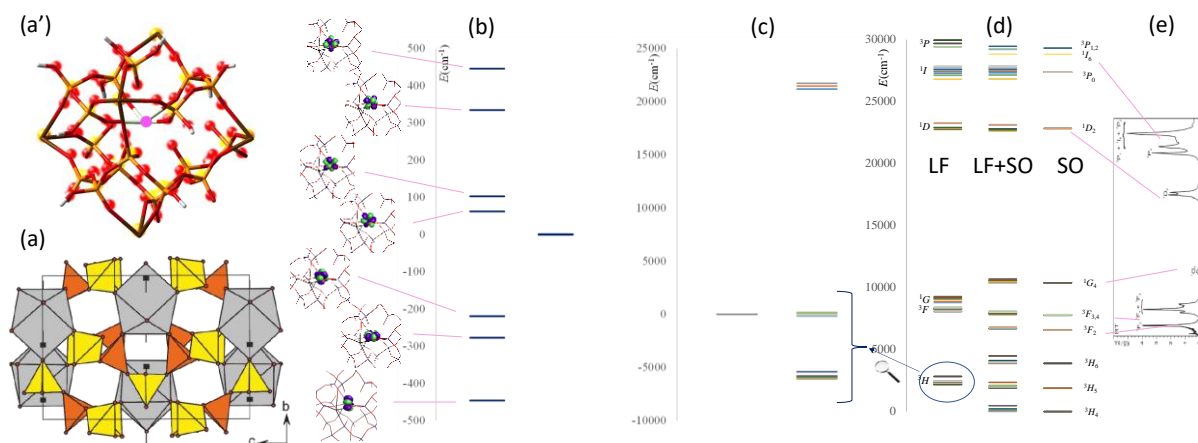
Figure 8. The PrP$_5$O$_{14}$ system: (a) crystal packing; (a') cropped cluster; (b) energies and shapes of calculated f orbitals (i.e. Ligand Field scheme, LF); (c) LF splitting of the fundamental term, ^{3}H; (d) LF splitting combined with spin-orbit (SO) effects calculated for the cluster from a'; (e) thumbnail of the experimental spectrum.

A case study of this type, the PrP$_5$O$_{14}$system, of the ultra-phosphate type, was approached following the discussions held with Professor Robert Glaum (renown specialist in spectroscopic experiments and Ligand Field modeling), on the sidelines of a specialized conference. The network contains infinite polymer filaments of phosphate units. However, a medium-sized (nearly nano-scale) fragment can be cut out. The summary of the data is given in figure 8. We performed the CASSCF treatment of this molecular cluster, including the spin-orbit (SO) coupling, thus achieving - thus - the principal realism possible in the interpretation and simulation of spectroscopic data. The methodological difficulties involved in this case were solved immediately, through innovative methods previously developed in our group.

A technical problem was given by the size of this system, which requires large memory resources and computing time. The results of the CASSCF calculation reach a reasonable fit with the experimental data of the lower spectral terms, but produce a sensitive overestimation of the higher ones, as can be seen from the comparison of boxes (d) and (e) in Figure 8. To identify the source of this imbalance, we put to point systematic tests, finding the cause in the orbital basis used for the Pr ion, otherwise a well-rated one, in principle (SARC-ZORA), including relativistic effects.

Testing an extended set of orbital bases we found that they all exhibit this tendency, by overestimating the Slater-Condon parameters, especially F_2^{ff}. The deep reason is probably the compensation effect that occurs during the optimization of the atomic fundamental energy (the usual way of producing basis sets), a slightly contracted radial profile attracting the concomitant increase of electron-electron repulsion and electron-nucleus attraction. To overcome this impediment we should produce a new basis set ourselves, also testing the performances in the field of excited states. Such an approach is within the know-how spectrum of our group, being - thus very tempting, but could not be resolved at this stage. At the same time, overcoming this small impediment is a condition for the completion of the cooperation attempt with Professor Glaum's group, through good experiment-theory corroboration, this desired being carried over to the next stage of the project.
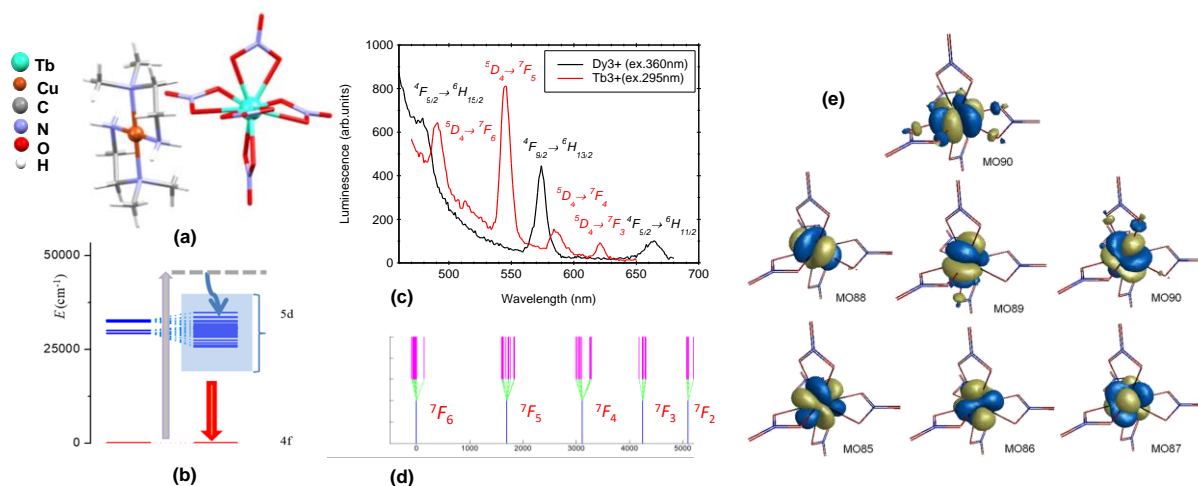
Figure 9. a) The molecular structure for [Cu(dmen)$_2$][Tb(NO$_3$)$_5$] compound resolved by single crystal X-ray diffraction. (b) The mechanism of luminescence in through d→f relaxation. (c) Experimental luminiscence spectra. (d) Calculation of the CASSCF-SO splitting for the ^7F term, the experimental data of the ^7F_J multiplets for the [Tb(NO$_3$)$_5$]$^{-2}$ unit. (e) The canonical molecular orbitals calculated by the CASSCF method for the same unit.

Another system approached on the path of multiconfigurational methods is the coordination compound sketched in Figure 9. This compound, of complex cation-complex anion type, was synthesized by our collaborators, aiming at the realization of a coordination sphere as simple as possible and at the same time independent, with effects packaging and long-range presumably as reduced as possible. The coordination unit][Tb(NO$_3$)$_5$]$^{2-}$ fulfills these requirements, allowing the systematic investigation of the competing components, in the calculation. The spectral simulation shown in the lower part of box (d) of Figure 9 is in good agreement with the experimentally recorded profile, shown in the upper part of panel (d).

4. Towards a new generation of ligand field models. (O4-part 1).

We propose a generalized form of the Ligand Field Hamiltonian (LF- Ligand Field) by "reverse engineering", assuming that the values and eigenvectors of the considered problem are known, ab initio way:

$$\hat{H}_{eff} = \sum_i |\psi_i\rangle \varepsilon_i \langle\psi_i| \qquad . \tag{5}$$

As a first hypothesis, we will consider as eigenvalues the orbital energies resulting from the calculations, ε_i, and as related eigenvectors, the molecular orbitals ψ. Noting the terms for the metal center and the ligand separately, by μ and λ, respectively, we write the functions of the LF sequence as follows:

$$\psi_i(x,y,z) = \sum_{M\in metal\ ion} c_{iM} \cdot \mu_M(x,y,z) + \sum_{L\in ligands} c_{iL} \cdot \lambda_L(x - X_L, y - Y_L, z - Z_L) . \tag{6}$$

The atomic components are Gaussian type orbitals (GTOs). These types of orbitals are treated in the format of the local Cartesian coordinates (x,y,z) of each atom, but they can also be formally expressed in the equivalent polar coordinates (r,θ,φ). Thus, we can dichotomize the atomic components into radial and angular parts: $\chi(x,y,z) \equiv \chi(r,\theta,\varphi) = R(l,\zeta,r) \cdot Z_{lm}(\theta,\varphi)$. The Z_{lm} notation represents the conversion of Y_{lm} complex spherical harmonics to real forms. The radial part of the GTO is

$$R(l,\zeta,r) = \mathcal{N}(l,\zeta) \cdot r^l \, exp(-\zeta \cdot r^2) \, ; \mathcal{N}(l,\zeta) = 2^{\frac{2l+5}{4}} \zeta^{\frac{2l+3}{4}} / \sqrt{\Gamma(l+3/2)} \, , \tag{7}$$

where Γ is the generalized factorial function for real variables (Gamma function).

To obtain an LF-type operator, the molecular orbitals ⊚i must be integrated on radial coordinates, taking the metal ion as the origin. As a first approximation, only the atomic orbitals of the metal atom can be considered, since they are usually the main part of the LF-type molecular functions. In this case, the integration can be done analytically, obtaining a generalized LF operator:

$$V_{LF}^M(\theta,\varphi) = \sum_{M_1} \sum_{M_2} \varepsilon_i \, c_{iM_1} c_{iM_2} \cdot S_{M_1,M_2} \cdot Z_{l_{M_1} m_{M_1}}(\theta,\varphi) Z_{l_{M_2} m_{M_2}}(\theta,\varphi) \,, \tag{8}$$

$$S_{M_1,M_2} \equiv S\big(l_{M_1},\zeta_{M_1},l_{M_2},\zeta_{M_2}\big) = \int_{r=0}^{\infty} R\big(l_{M_1},\zeta_{M_1},r\big) \cdot R\big(l_{M_2},\zeta_{M_2},r\big) r^2 dr \,, \tag{9}$$

$$(l_1,\zeta_1,l_2,\zeta_2) = \tfrac{1}{2}\mathcal{N}(l_1,\zeta_1)\mathcal{N}(l_2,\zeta_2) \cdot \Gamma\left(\tfrac{l_1+l_2+3}{2}\right) / (\zeta_1+\zeta_2)^{\frac{l_1+l_2+3}{2}} \,. \tag{10}$$

The product of two spherical harmonics with quantum numbers l_1 and l_2 can be developed as a sum of spherical functions running between $|l_1 - l_2|$ and l_1+l_2. In principle, the analytical expansion can also be performed with the ligand parts included, but, for practical reasons, we resorted to numerical integration. Thus, we borrowed a technique used in producing pseudo-potentials used in solid-state calculations. The idea is to express a radial integral as a sum over a fixed set of points, factored by specific weights:

$$\int_{r=0}^{\infty} f(r)dr \approx \sum_{m=1}^{n_{max}} w_m \cdot f(r_m) \,. \tag{11}$$

We used a denser grid of points at the origin, which thins out as the distance from the origin increases:

$$r_m = \delta r_0 \frac{exp(mh)-1}{exp(h)-1} \,, \quad w_m = h \cdot \delta r_0 \frac{exp(kh)}{exp(h)-1} \,,'' \tag{12}$$

with δr_0 =0.001 Bohr and h=0.0211, obtaiing n_{max} =254 and r_{max}=10 Bohr. The functions subjected to numerical integration by the previously described equation can be written, for the metal-ligand terms, as follows:

$$f(r) = R(l_M,\zeta_M,r) \cdot R(l_L,\zeta_L,|\boldsymbol{r} - \boldsymbol{R_L}|) \cdot Y_{LM}^{real}(\theta_L,\varphi) \tag{13}$$

where $\boldsymbol{R_L}$ marks the position of the ligand L atom. The representation of L centers causes the spherical harmonics on them to acquire a dependence on the radial part, from the referential of the central ion. The ligand-ligand terms can be neglected, due to their small coefficients and the practically zero overlap of their radial functions.

The finality of the scheme is achieved by expressing the numerical results by fitting as a series of spherical harmonic functions::

$$\hat{V}_{LF}(\theta,\varphi) = \sum_{k=k_{min}}^{k_{max}} \sum_{q=-k}^{k} B_q^k Z_{k,q}(\theta,\varphi) \,, \tag{14}$$

The generalization consists in the fact that we allow a wide spectrum of spherical functions, from k_{min}=1 to k_{max} =10. The traditional LF models are limited, for empirical-phenomenological reasons, only to the sets k =2, 4 and 6. With a wide spectrum of spherical functions, we obtain an overdetermined system of linear equations: $\boldsymbol{\mathcal{A}} \cdot \boldsymbol{b} = \boldsymbol{u}$, where the coefficients to be fitted are the generalized LF parameters, B_k^q, concatenated in a single column, for k successive sets: $b_{k^2+k+q} \equiv b_{k^2+k+q,1} = B_k^q$.

The data that feed the problem are the values of the potential estimated on a grid of polar coordinates $\{\theta_i, \varphi_j\}$, reordered by concatenating the lines of the vij matrix (the particularizations of the potential from equation 14 in the grid coordinates) in a single column: $u_{N_\varphi \cdot (i-1)+j} \equiv u_{N_\varphi \cdot (i-1)+j,1} = v_{ij}$. The structure factors are obtained by estimating the entire set of real spherical harmonics at the polar coordinate grid, arranged in the following matrix: $\mathcal{A}_{N_\varphi \cdot (i-1)+j,k^2+k+q} = Z_{kq}(\theta_i,\varphi_j)$. In the given setting, there are 1200 v_{ij} points and 120 B_k^q coefficients of spherical harmonics, from k_{min} =1 to k_{max} =10. The solution, according to the method of least squares, is obtained by pseudo-inverse:

$$\boldsymbol{b} = \boldsymbol{\mathcal{A}}^{\#} \cdot \boldsymbol{u}, \quad \boldsymbol{\mathcal{A}}^{\#} = \big(\boldsymbol{\mathcal{A}}^T \cdot \boldsymbol{\mathcal{A}}\big)^{-1} \cdot \boldsymbol{\mathcal{A}}^T. \tag{15}$$

This analysis can be applied to calculated potential or data limited to metal ion contributions only. In addition, one can try fitting on the limited sets of spherical harmonics used in the traditional LF formulas, namely k=2 and 4 for d-type elements ([FeF$_3$] system) or k=2, 4 and 6 for f-type (case [GdF$_3$]). Figure 10 shows the concatenated lists of B_k^q coefficients with k ranging from 1 to 10 and, within each range k, q running from -k to k, k^2+k+q being the order number (rendered in logarithmic scale) assigned to the parameter B_k^q.
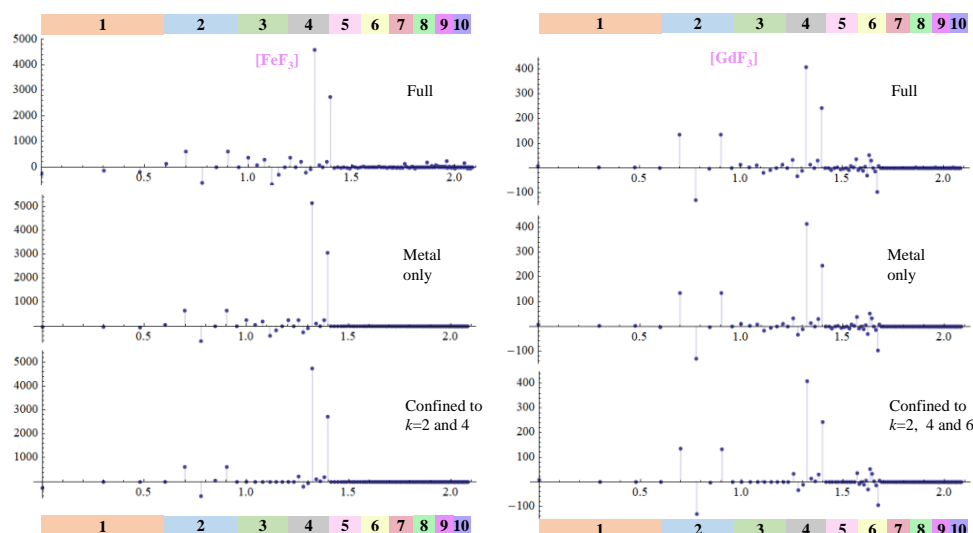

Figure 10. The fit of the computed LF effective Hamiltonian for [FeF$_3$] and [GdF$_3$] numeric experiments with a generalized range of spherical harmonics components, with k ranging from 1 to 10. The values of B_k^q parameters are shown by vertical bars, while the abscissa shows their ordering, first by k then q, and the resulting position is shown on a logarithmic scale. The k ranges are marked below and above the histograms. The top insets contain results of the full effective potentials, with metal and ligand terms. The middle panels show the approximation to metal-based components only. The bottom shows the limitation of the k set, like in traditional LF models.

The graphs in the lower part contain the results of fitting within the limits of the standard models, the upper ones the extended modeling, described above, and the middle ones, the results of an intermediate approximation, limiting the harmonic sets between k=1 and 6. Although the main components already appear from the basic level of the standard models, the extended approach shows the relative relevance of the higher terms. The scheme can be extended beyond the approach approached here, as the simplest direction, of assimilating the LF scheme with energies and orbital functions. The next step would consist in the extension of the method to polyelectronic states, integrated corresponding to the generation of an effective mooelectron potential, assignable to the field of the ligands. At the same time, it would be necessary to verify whether this path can, alternatively, be fed with data obtained by exploring the density data from band calculation, similar to the investigations described in the first section.

*
**
***
*****